Fabrication of Eu3 + and Sm3 + Codoped Micro/Nanosized MMoO4 (M= Ca, Ba, and Sr) via Facile Hydrothermal Method and Their Photoluminescence Properties Through Energy Transfer

ARTICLE *in* THE JOURNAL OF PHYSICAL CHEMISTRY C · MARCH 2008

Impact Factor: 4.77 · DOI: 10.1021/jp800559f

Fabrication of Eu^{3+} and Sm^{3+} Codoped Micro/Nanosized $MMoO_4$ (M = Ca, Ba, and Sr) via Facile Hydrothermal Method and Their Photoluminescence Properties through Energy Transfer

Ye Jin,[†,‡] Jiahua Zhang,*[,†] Shaozhe Lü,[†] Haifeng Zhao,[†] Xia Zhang,[†] and Xiao-jun Wang*[,†,§]

Key Laboratory of Excited State Processes, Changchun Institute of Optics, Fine Mechanics and Physics, Chinese Academy of Sciences, 16 Eastern South Lake Road, Changchun 130033, China; Graduate School of Chinese Academy of Sciences, Beijing 100039, China; and Department of Physics, Georgia Southern University, Statesboro, Georgia 30460

Received: January 17, 2008; In Final Form: February 27, 2008

Eu^{3+} and Sm^{3+} codoped micro/nanosized $MMoO_4$ (M = Ca, Ba, Sr) phosphors with various shapes have been synthesized via a facile hydrothermal method with surfactant-free environment. The morphology of the materials was found to be manipulated by the pH value of the precursor solution. $MMoO_4$:Eu^{3+}, Sm^{3+} (M = Ca, Ba, Sr) nanoflakes, microflowers, cubes, and spheres were obtained and characterized by X-ray diffraction and field emission scanning electron microscopy. The luminescent properties of the molybdate phosphors were systematically studied. The introduction of Sm^{3+} into each of the red-emitting phosphors $MMoO_4$:Eu^{3+} (M = Ca, Ba, Sr) can generate a strong excitation line at 405 nm, originating from the $^6H_{5/2} \rightarrow {}^6P_{5/2}$ transition of Sm^{3+}, significantly extending the excitation region for matching the near-ultraviolet light-emitting diodes (~400 nm). Energy transfer from Sm^{3+} to Eu^{3+} was observed in the whole $MMoO_4$ systems and investigated in detail in $CaMoO_4$ as a function of Sm^{3+} concentrations. A back-energy transfer was also evidenced by the shortening of the $^5D_0$ lifetimes of Eu^{3+} with increasing Sm^{3+} concentrations.

1. Introduction

Self-assembled microstructure and nanostructures with specific morphology and novel physical and chemical properties have attracted great attention in recent years, owing to their potential applications as advanced materials in the future.[1,2] Lots of one-dimensional (1D), two-dimensional (2D), and three-dimensional (3D) assembled superstructures have been synthesized by using various methods.[3,4] Among them, the frequent one is the surfactant-assistant method, with which a surfactant with other solutions forms oil-in-water or water-in-oil microemulsion to control the morphology of the products.[5,6] However, there are some points which cannot be neglected: (1) a surfactant is usually organic material which is not good for luminescence; (2) the utilization of the surfactant is a complicated process that restricts the popularization of the techniques in practical applications, and the important one is that it will increase the production cost. So it is a significant work to find a template-free method which is useful in synthesizing of the assembled 1D, 2D, or 3D structures.

Molybdate with a sheelite-type structure has been of practical interest for a long time because of its attractive luminescence property with the promising applications in photoluminescence, optical fibers, and scintillators.[7−11] Recently, Eu^{3+} doped $CaMoO_4$ has been investigated extensively as a red-emitting phosphor for near-ultraviolet (UV) GaN chip (390−410 nm) based white-light-emitting diodes (W-LEDs).[12,13] This phosphor demonstrates strong red fluorescence, originating from $^5D_0 \rightarrow {}^7F_2$ transition of Eu^{3+} upon near-UV excitation into the $^5L_6$ state of Eu^{3+} at 395 nm. It also exhibits more stable physical and chemical properties than the well-known red phosphor, Y_2O_2S:Eu^{3+}, and no concentration quenching.[14,15] A few significant investigations have been done to further improve the luminescent properties of this phosphor by codoping other metal ions. In our previous work, the luminescent enhancement of Eu^{3+} in $CaMoO_4$ was observed by codoping Bi^{3+}.[16] To extend the near-UV excitation lines for effectively covering the near-UV LED source in the spectral range, Sm^{3+} was codoped into $CaMoO_4$:Eu^{3+}.[17] In this case, energy transfer between Sm^{3+} and Eu^{3+} occurs, resulting in the appearance of a new excitation line at 405 nm, originating from $^6H_{5/2} \rightarrow {}^6P_{5/2}$ transition of Sm^{3+}. The study on dynamical processes in energy transfer between Sm^{3+} and Eu^{3+} in $MMoO_4$ (M = Ca, Sr, Ba), however, has not been demonstrated. In this paper, we systematically report the synthesis and luminescent properties of the nano- and microsized $MMoO_4$:Eu^{3+}, Sm^{3+} (M = Ca, Sr, Ba) system. 2D $CaMoO_4$:Eu^{3+}, Sm^{3+} nanoflakes and its self-assembly into microflowers in surfactant-free environment, $SrMoO_4$:Eu^{3+}, Sm^{3+} microspheres, and $BaMoO_4$:Eu^{3+}, Sm^{3+} microflowers are demonstrated. The energy transfer in $CaMoO_4$:Eu^{3+}, Sm^{3+} is mainly studied by analyzing the change of excitation spectra and fluorescence lifetimes of Eu^{3+} with different Sm^{3+} concentrations. The optimal composition of $CaMoO_4$:20% Eu^{3+}, 3% Sm^{3+} is finally determined.

2. Experimental Section

The nanostructure and microstructure $MMoO_4$ (M = Ca, Sr, Ba) were synthesized via a facile hydrothermal method. The required device is a 50 mL Teflon-lined stainless steel autoclave. All the raw chemical materials were used without further

* Corresponding authors: Tel/Fax +86-431-8617-6317; e-mail zhangjh@ciomp.ac.cn or xwang@georgiasouthern.edu.
† Changchun Institute of Optics, Fine Mechanics and Physics, Chinese Academy of Sciences.
‡ Graduate School of Chinese Academy of Sciences.
§ Georgia Southern University.

10.1021/jp800559f CCC: $40.75
Published on Web 03/27/2008

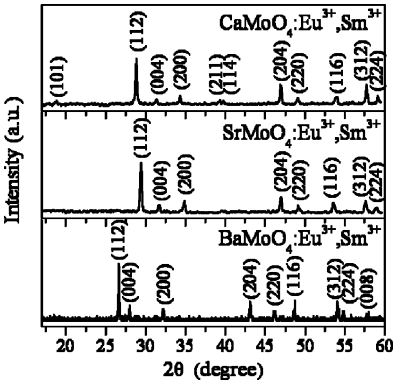

Figure 1. XRD patterns of Eu^{3+} and Sm^{3+} codoped $MMoO_4$ (M = Ca, Sr, Ba) materials.

purification. The detail of reaction procedure is as follows: $Na_2MoO_4 \cdot H_2O$ was used to offer MoO_4^{2-}, and it was prepared by adding 2 mmol of $Na_2MoO_4 \cdot H_2O$ into 20 mL of deionized water. Meanwhile, 2 mmol of MO (M = Ca, Sr, Ba) was solved in 20 mL of thin nitrate to be $M(NO_3)_2$ solution. Then, the dopant ions were added into $M(NO_3)_2$ solution by dropping appreciated $Eu(NO_3)_3$ (0.1 M) or $Sm(NO_3)_3$ (0.01 M) solution, which was prepared in advance. The Na_2MoO_4 solution was dropped into $M(NO_3)_2$:Eu^{3+}, Sm^{3+} solution slowly under vigorous stirring. A white precipitate was observed in the glass beaker. The pH value was adjusted to an appropriate constant with diluted ammonia or diluted nitric acid, which is a key factor to the morphology of the product. The vigorous stirring was continued for 30 min. Finally, the precursor solution was transferred into a 50 mL Teflon-lined stainless steel autoclave, which was subsequently sealed and maintained at 130 °C for 6 h. After that, the autoclave was cooled to room temperature naturally. The product was collected by filtering and washing several times with deionized water and absolute ethanol. Then, the powder was obtained after being dried in air at 100 °C for 2 h.

The structures of samples were characterized by X-ray diffraction (XRD) (Rigaku D/max-rA powder diffractometer with Cu target radiation resource (λ = 1.540 78 Å)). The morphology was investigated by using field emission scanning electron microscopy (FE-SEM) (Hitachi S-4800). Fluorescence and excitation spectra were recorded at room temperature using a Hitachi F-4500 spectrophotometer equipped with a 150 W Xe-arc lamp. The emission spectra were measured at a fixed band-pass of 0.2 nm with the same instrument parameters. Luminescent decay curves were recorded by an oscillograph (Tektronix, TDS 3052, 500 MHz, 5 Gs/s), with a 266 nm light as excitation source. It was generated from the fourth-harmonic generator pumped by the pulsed Nd:YAG laser, with a line width of 1.0 cm^{-1}, pulse duration of 10 ns, and repetition frequency of 10 Hz.

3. Results and Discussion

The structures of the samples were characterized by XRD patterns, which are shown in Figure 1. The XRD patterns of $CaMoO_4$:20% Eu^{3+}, 2% Sm^{3+}, $BaMoO_4$:20% Eu^{3+}, 2% Sm^{3+}, and $SrMoO_4$:20% Eu^{3+}, 2% Sm^{3+} are consistent with JCPDS No. 29-0193, No. 08-0482, and No. 85-0585, respectively. All the reflection peaks were labeled in Figure 1. No additional peaks can be found in the patterns, indicating that the dopant ions did not change the structure of hosts.

Figure 2 shows the typical SEM images of $CaMoO_4$:Eu^{3+}, Sm^{3+} samples prepared in different reaction conditions. Figure

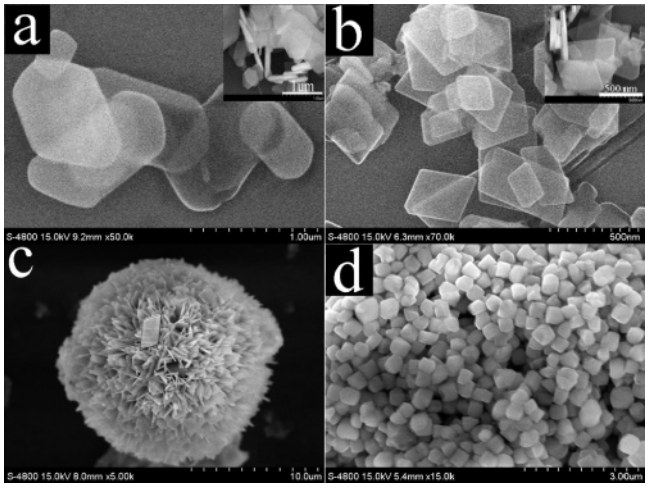

Figure 2. Typical SEM images of $CaMoO_4$:20% Eu^{3+}, 2% Sm^{3+} under different conditions. (a) pH ~ 3−4 of the precursor solution. (b) pH ~ 4−5. (c) pH ~ 5−6. (d) The sample shown in (b) after annealing at 200 °C for 4 h.

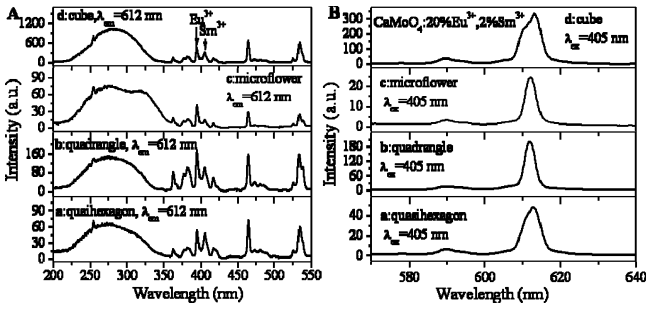

Figure 3. Room temperature excitation (A) and emission (B) spectra of $CaMoO_4$:20% Eu^{3+}, 2% Sm^{3+} with different shapes.

2a is the quasi-hexagonal $CaMoO_4$:Eu^{3+}, Sm^{3+} nanoflakes with 500 nm width and 100 nm thickness (inset), which were obtained in the precursor solution with pH value around 3−4. When the pH value was adjusted to 4−5, the morphology was quadrangle with about 500 nm width and 50 nm thickness, as shown in Figure 2b. As the pH value was adjusted to 5−6, a flowerlike shape was obtained, as shown in Figure 2c. Figure 2d shows the cubes converted from the quadrangles shown in Figure 2b after annealing at 200 °C for 4 h. From all the images of Figure 2, the thickness of all the flakes is almost uniform around 100 nm, and the nanoflakes are linked together by either edge-to-edge or edge-to-surface conjunction.

In our experiment, it was found that the pH value of the precursor solution plays a crucial role in shape and size controlling of these building subunits. The shapes of flakes can be restricted by pH value of the precursor, and it is also affected whether the flakes aggregated to flowerlike products.

Figure 3A,B illustrates the excitation and emission spectra of these $CaMoO_4$:20% Eu^{3+}, 2% Sm^{3+} samples with different shapes, as illustrated in Figure 2. The excitation spectra monitoring the red emission line at 612 nm are composed of an intense broad band and some sharp lines. The broad band in the range of 200−350 nm is assigned to the combination of the charge-transfer transition of $O^{2-} \rightarrow Mo^{6+}$ and $O^{2-} \rightarrow Eu^{3+}$. For the microflower sample, it can be seen that a new broad excitation band appears at 325 nm. The sharp line around 405 nm corresponds to the $^6H_{5/2} \rightarrow {}^6P_{5/2}$ transition of Sm^{3+},[17] and the other sharp lines including the strong one at 395 nm correspond to the transitions of Eu^{3+} ions. The appearance of the 405 nm excitation line indicates the performance of energy transfer from Sm^{3+} to Eu^{3+}.

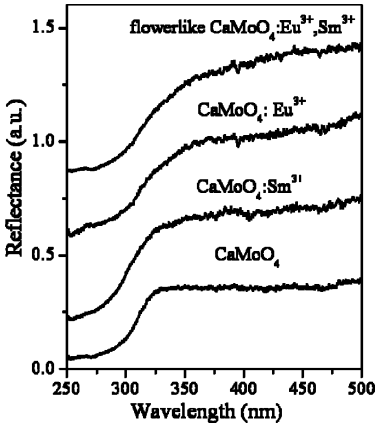

Figure 4. Reflection spectra of $CaMoO_4$ host and rare earth doped $CaMoO_4$.

The diffused reflectance spectra of the samples with different dopant ions were measured, as shown in Figure 4. An absorption edge at 300 nm owing to MoO^{2-} is clearly presented in all the samples, and the Eu^{3+} absorption peaks corresponding to $^7F_0 \rightarrow {}^5L_6$ transition at 395 nm, $^7F_0 \rightarrow {}^5D_2$ transition at 465 nm, and Sm^{3+} $^6H_{5/2} \rightarrow {}^6P_{5/2}$ transition at 405 nm are also observed. It can be found that the Eu^{3+}-free samples exhibit a sharp absorption edge, and the Eu^{3+} doped samples, however, show additional absorbance in the range of 300−350 nm, making the absorption edge very slow. In view of the results of the diffused reflectance spectra, the additional broad excitation band at 325 nm in microflower $CaMoO_4$:20% Eu^{3+}, 2% Sm^{3+} is considered to be related to Eu^{3+}. In molybdates, the changes of O → Mo CTB owing to the influence of Eu^{3+} ions were also reported in the literature.[13]

Characteristic emission peaks of Eu^{3+} within the wavelength range from 580 to 620 nm, corresponding to the transitions from the excited $^5D_0$ to ^7F_J ($J = 1, 2$) levels, were observed in the emission spectra (Figure 3B). The relative intensities of the $^5D_0 \rightarrow {}^7F_2$ transition to $^5D_0 \rightarrow {}^7F_1$ emission range from 3.6 to 7.2; that of cubic $CaMoO_4$:Eu^{3+}, Sm^{3+} is the strongest, and that of the flowerlike one is the weakest. The emission of Sm^{3+} ions did not appear even under direction excitation of Sm^{3+}. It means the occurrence of efficient energy transfer from Sm^{3+} ions to Eu^{3+} ions. A possible four-step energy transfer mechanism from Sm^{3+} ions to Eu^{3+} ions has been elaborated.[17] It was described that the electron was excited from the ground state $^6H_{5/2}$ to $^6P_{5/2}$, and it jumped down to $^5G_{5/2}$ of Sm^{3+} ions and transferred to $^5D_0$ state of Eu^{3+} ions nonradiatively. Thus, the emission of $^5D_0 \rightarrow {}^7F_2$ transition of Eu^{3+} ions was observed.

From Figure 3A,B, the most intense luminescence is from the cubic $CaMoO_4$:20% Eu^{3+}, 2% Sm^{3+} under 405 nm excitation. It means that the energy transfer in cubic $CaMoO_4$:20% Eu^{3+}, 2% Sm^{3+} is the most efficient. The most probable reason is that the sample had been annealed at 200 °C for 4 h, which may eliminate many defects that block the energy transfer between Sm^{3+} and Eu^{3+}.

For the energy transfer between Sm^{3+} ions and Eu^{3+} ions, the investigation in $CaMoO_4$ host with microflower shape in detail has been done, and the excitation and emission spectra are shown in parts A and B of Figure 5, respectively. Excitation spectra were recorded by monitoring the emission of Eu^{3+} ions at 612 nm, and emission spectra were performed under 405 nm excitation. In $CaMoO_4$, the concentration of Eu^{3+} ions was fixed at 20%, and the concentrations of Sm^{3+} ranged from 0 to 5%. In the excitation spectrum of Eu^{3+} singly doped $CaMoO_4$ in the near-UV range of 390−410 nm, only a strong line at 395 nm appears. The introduction of Sm^{3+} into $CaMoO_4$:Eu^{3+} generates an excitation line at 405 nm. The excitation peaks at 395 nm and at 405 nm grow with the increasing of the Sm^{3+} concentrations up to 3% and then decrease as the Sm^{3+} concentration beyond 3%. As a result, it is speculated that there exists a back-energy transfer from Eu^{3+} to Sm^{3+}.

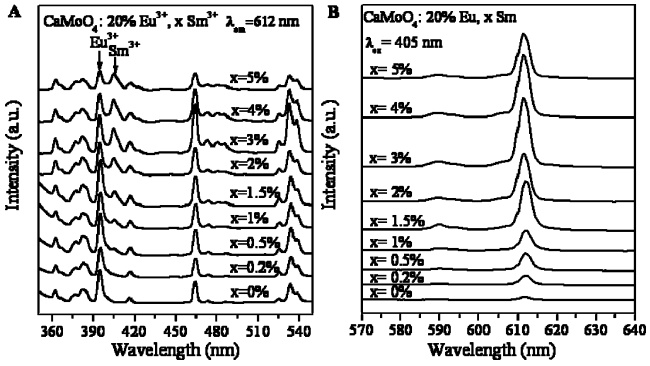

Figure 5. Excitation (A) and emission (B) spectra of $CaMoO_4$:20% Eu^{3+}, x Sm^{3+} ($x = 0-5\%$).

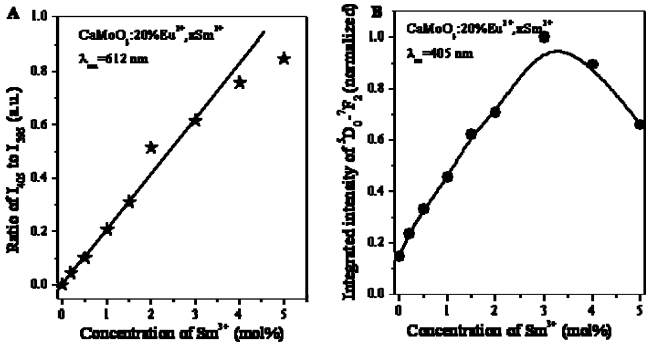

Figure 6. Dependence of ratio of I_{405} to I_{395} and integrated intensity of $^5D_0 \rightarrow {}^7F_2$ transition of Eu^{3+} ions on the concentration of Sm^{3+} ions in $CaMoO_4$ ($\lambda_{ex} = 405$ nm).

The intensity ratios of the 405 nm peak to the 395 nm peak (I_{405}/I_{395}) increase monotonously with increasing the Sm^{3+} concentrations, demonstrating enhanced energy transfer efficiency, as shown in Figure 6A. The dependence of the ratio of I_{405}/I_{395} on the concentration of Sm^{3+} ions is close to a linear relationship as Sm^{3+} concentration lower than 3%. When the product was under continuous excitation into Sm^{3+} at 405 nm, we have the following equations:

$$f\sigma_1 c_1 = \gamma_1 n_1 + W_{12} n_1 c_2 - W_{21} n_2 c_1 \quad (1)$$

$$W_{12} n_1 c_2 = \gamma_2 n_2 + W_{21} n_2 c_1 \quad (2)$$

where f is the excitation density; σ_i, c_i, γ_i, and n_i are absorption cross section, doping concentration, relaxation rate, and excited-state populations, respectively, for dopant i ($i = 1$ for Sm^{3+} and 2 for Eu^{3+}); W_{12} and W_{21} denote the energy transfer coefficients from Sm^{3+} to Eu^{3+} and back-transfer from Eu^{3+} to Sm^{3+}, respectively. From eqs 1 and 2, one has

$$n_2 = \frac{f\sigma_1 c_1 W_{12} c_2}{\gamma_1\gamma_2 + \gamma_1 W_{21} c_1 + W_{12} c_2 \gamma_2} \quad (3)$$

Similarly, when Eu^{3+} is continuously excited by 395 nm, we have the two equations

$$f\sigma_2 c_2 = \gamma_2 n_2' + W_{21} n_2' c_1 - W_{12} n_1' c_2 \quad (4)$$

$$W_{21}n_2'c_1 = \gamma_1 n_1' + W_{12}n_1'c_2 \quad (5)$$

From eqs 4 and 5, the population of Eu^{3+} is written as

$$n_2' = \frac{f\sigma_2 c_2(\gamma_1 + W_{12}c_2)}{\gamma_1\gamma_2 + \gamma_2 W_{12}c_2 + \gamma_1 W_{21}c_1} \quad (6)$$

The ratio is

$$\frac{I_{405}}{I_{395}} = \frac{n_2}{n_2'} = \frac{\sigma_1 c_1 W_{12}}{\sigma_2(c_2 W_{12} + \gamma_1)} \quad (7)$$

Therefore, the ratio of I_{405}/I_{395} is basically a linear dependence on c_1, the concentration of Sm^{3+} ions. From eq 7, a linear dependence of I_{405}/I_{395} on c_1 is expected if γ_1 is independent of c_1. Figure 6A, however, demonstrates a deviation from linear dependence as Sm^{3+} concentration higher than 3%. It is considered that the energy diffusion among Sm^{3+} is rapidly speeded up with increasing Sm^{3+} concentrations and thus dominates the relaxation rate, γ_1, at higher Sm^{3+} concentrations.

Figure 6B shows the dependence of luminescence intensity on Sm^{3+} concentrations upon 405 nm excitation in $CaMoO_4$: 20% Eu^{3+}, 3% Sm^{3+}. It can be seen the luminescence reaches the maximum at Sm^{3+} concentration of 3%. From eq 3, the continued increasing of Sm^{3+}concentration c_1 can possibly cause the maximum intensity of n_2 due to γ_1 in the denominator of eq 3. The optimal composition of $CaMoO_4$:20% Eu^{3+}, 3% Sm^{3+} is finally determined.

The back-energy transfer was studied by measuring the lifetimes of the Eu^{3+} emission at 612 nm as a function of Sm^{3+}-concentration, shown in Figure 7. When the concentration of Sm^{3+} ions was lower than 3%, the lifetimes of Eu^{3+} ions change slowly. As the concentration was more than 3%, the lifetime was obviously shortened, indicating the effect of back-transfer from the $^5D_0$ level of Eu^{3+} to the $^4G_{5/2}$ level of Sm^{3+}.

$BaMoO_4$:Eu^{3+}, Sm^{3+} microflowers and $SrMoO_4$:Eu^{3+}, Sm^{3+} microspheres have been also synthesized by adjusting pH value to 3 and 5, respectively. Under the same hydrothermal condition as that of $CaMoO_4$:Eu^{3+}, Sm^{3+}, the morphology of $BaMoO_4$: Eu^{3+}, Sm^{3+} is also microflowers, similarly to that of $CaMoO_4$: Eu^{3+}, Sm^{3+}, except the size growing up, while the shape of $SrMoO_4$:Eu^{3+}, Sm^{3+} is 800 nm diameter microspheres, as displayed in Figure 8. Figure 8a is the low-magnification SEM image of $BaMoO_4$:Eu^{3+}, Sm^{3+}, and Figure 8b is high-magnification SEM image, which suggests that the flakes composed of microflower are some anomalous flakes. Figure 8c is the general view of the product $SrMoO_4$:Eu^{3+}, Sm^{3+}, suggesting that most of the product is microspheres. Figure 8d depicts the high magnification of the spherical $SrMoO_4$:Eu^{3+}, Sm^{3+}, and the diameter of $SrMoO_4$:Eu^{3+}, Sm^{3+} is about 800 nm.

Figure 9 shows the excitation and emission spectra of $MMoO_4$:20% Eu^{3+}, 2% Sm^{3+} (M = Ca, Sr, Ba). As can be seen, the 405 nm excitation line also appears in $BaMoO_4$:Eu^{3+}, Sm^{3+} and $SrMoO_4$:Eu^{3+}, Sm^{3+}, indicating the performance of energy transfer from Sm^{3+} to Eu^{3+}. While both the emission at 612 nm and the excitation band at 325 nm grow up with changing host in the order of $BaMoO_4$, $SrMoO_4$, and $CaMoO_4$, in molybdates the central Mo^{6+} metal ion is coordinated to four oxygen atoms in tetrahedral symmetry (T_d) and the cations with eight oxygen atoms form different tetrahedrons. The ionic radii of Eu^{3+} (r = 1.07 Å when coordination number (CN) = 8) and Sm^{3+} are close to that of Ca^{2+} (r = 1.12 Å when CN = 8) rather than those of Sr^{2+} (r = 1.20 Å when CN = 8) and Ba^{2+}

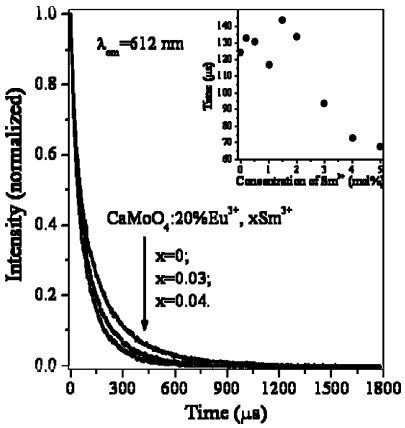

Figure 7. Room temperature luminescent decay curves of $^5D_0 \rightarrow {}^7F_2$ transitions at 612 nm of Eu^{3+} ions of $CaMoO_4$:20% Eu^{3+}, x Sm^{3+} (x = 0−5%). Inset: dependence of the lifetime at 612 nm of Eu^{3+} ions on the concentration of Sm^{3+} ions in $CaMoO_4$.

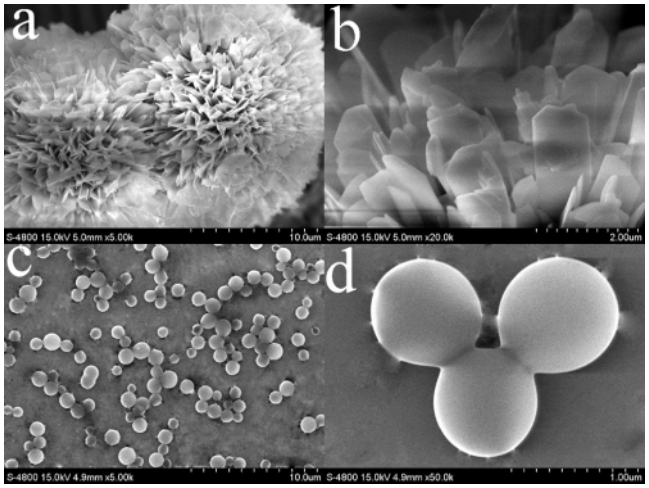

Figure 8. SEM images of $BaMoO_4$:Eu^{3+}, Sm^{3+} and $SrMoO_4$:Eu^{3+}, Sm^{3+}. SEM image of $BaMoO_4$:Eu^{3+}, Sm^{3+} in low magnification (a) and in high magnification (b). SEM image of $SrMoO_4$:Eu^{3+}, Sm^{3+} in low magnification (c) and in high magnification (d).

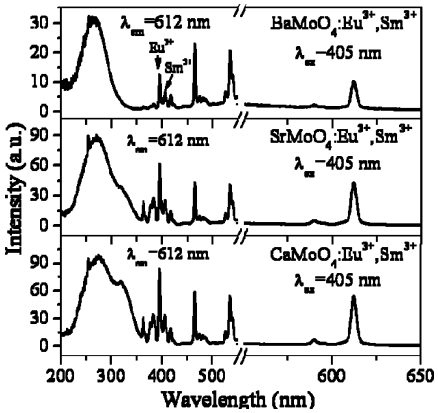

Figure 9. Excitation and emission spectra of $MMoO_4$:20% Eu^{3+}, 2% Sm^{3+} (M = Ca, Sr, Ba).

(r = 1.38 Å when CN = 8).[16] The lattice distortion due to substitution of Eu^{3+} and Sm^{3+} for M^{2+} (M = Ba, Sr, Ca) sites reasonably becomes smaller with M changing from Ba to Sr and Ca. The strongest luminescence and the excitation band at 325 nm in $CaMoO_4$, therefore, are expected.

The luminescent dynamics of Eu^{3+} ions in the three hosts have been also investigated. Figure 10 shows the fluorescence decay patterns in $CaMoO_4$:20% Eu^{3+}, 2% Sm^{3+}, $BaMoO_4$:20%

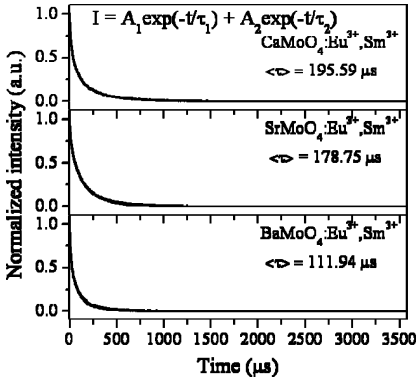

Figure 10. Room temperature luminescent decay curves of $^5D_0$ of Eu^{3+} ions of $MMoO_4$:20% Eu^{3+}, 2% Sm^{3+} (M = Ca, Sr, Ba).

Eu^{3+}, 2% Sm^{3+}, and $SrMoO_4$:20% Eu^{3+}, 2% Sm^{3+}. The decay curves are nonexponential and well fitted into a two-exponential function

$$I = A_1 \exp(-t/\tau_1) + A_2 \exp(-t/\tau_2)$$

where τ_1 and τ_2 are time constants and A_1 and A_2 are constants. The average lifetimes were calculated by using the formula

$$\langle \tau \rangle = \frac{A_1 {\tau_1}^2 + A_2 {\tau_2}^2}{A_1 \tau_1 + A_2 \tau_2}$$

As can be seen, the average lifetime in $CaMoO_4$:Eu^{3+}, Sm^{3+} was the longest and that in the $BaMoO_4$:Eu^{3+}, Sm^{3+} is the shortest. This result further reflects the effect of lattice distortion, which perhaps results in nonradiative relaxation channels and reduction of the $^5D_0$ lifetime in the three materials. The nonexponential decay can be also caused by the nonradiative relaxation channels with different rates or the back energy transfer from Eu^{3+} to Sm^{3+}.

4. Conclusions

In conclusion, $CaMoO_4$:Eu^{3+}, Sm^{3+} nanoflakes, microflowers, cubes, and $BaMoO_4$:Eu^{3+}, Sm^{3+} microflowers and $SrMoO_4$:Eu^{3+}, Sm^{3+} microspheres were synthesized systematically via facile hydrothermal method with surfactant-free environment. The pH value of the precursor was found to be a crucial factor to affect the morphology of the products. For $CaMoO_4$:Eu^{3+}, Sm^{3+}, when the pH value was adjusted to be 3−4, it is quasi-hexagon nanoflakes; when 4−5 and 5−6 they are quadrangles and microflowers, respectively. The red fluorescence of Eu^{3+} and energy transfer from Sm^{3+} to Eu^{3+} in all the products were observed. In $CaMoO_4$:20% Eu^{3+}, x Sm^{3+} (x = 0−5%), the ratio of I_{405}/I_{395}, related to energy transfer efficiency, increases linearly with the concentration of Sm^{3+} up to 3% and increases slowly as Sm^{3+} concentration higher than 3%, which is attributed to the effect of energy diffusion among Sm^{3+} ions. A back-energy transfer from Eu^{3+} to Sm^{3+} was also observed by measuring the fluorescence lifetimes of Eu^{3+} as a function of Sm^{3+}concentrations. Owing to efficient energy transfer, a strong excitation line at 405 nm, originating from $^6H_{5/2} \rightarrow {}^6P_{5/2}$ transition of Sm^{3+}, is generated in the excitation spectra of the Eu^{3+} fluorescence. It significantly extends the excitation region of these materials for matching the near-ultraviolet light-emitting diodes (∼400 nm). For the aim to use in W-LEDs with high color rendering index and color reproducibility, Eu^{3+} and Sm^{3+} codoped $MMoO_4$ (M = Ca, Sr, Ba) materials are good choices to afford red-emitting components.

Acknowledgment. This work was financially supported by the MOST of China (2006CB601104 and 2006AA03A138) and the National Natural Science Foundation of China (10774141 and 10574128).

References and Notes

(1) Wang, Z. L. *Adv. Mater.* **2003**, *15*, 432.
(2) Wang, X. D.; Song, J. H.; Liu, J.; Wang, Z. L. *Science* **2007**, *316*, 102.
(3) Zhang, G. Q.; Zhang, T.; Lu, X. L.; Wang, W. *J. Phys. Chem. C* **2007**, *111*, 12663.
(4) Gao, Y. H.; Bao, Y. P.; Beerman, M.; Yasuhara, A.; Shindo, D. *Appl. Phys. Lett.* **2004**, *84*, 3361.
(5) Gong, Q.; Qian, X. F.; Ma, X. D.; Zhu, Z. K. *Cryst. Growth Des.* **2006**, *6*, 1821.
(6) Sun, L.; Guo, Q.; Wu, X.; Luo, S.; Pan, W.; Huang, K.; Lu, J.; Ren, L.; Cao, M.; Hu, C. *J. Phys. Chem. C* **2007**, *111*, 532.
(7) Oi, T.; Takagi, K.; Fukazawa, T. *Appl. Phys. Lett.* **1980**, *36*, 278.
(8) Wang, H.; Medina, F. D.; Zhou, Y. D.; Zhang, Q. N. *Phys. Rev. B* **1992**, *45*, 10356.
(9) Tanaka, K.; Miyajima, T.; Shirai, N.; Zhuang, Q.; Nakata, R. *J. Appl. Phys.* **1995**, *77*, 6581.
(10) Liao, H. W.; Wang, Y. F.; Liu, X. M.; Li, Y. D.; Qian, Y. T. *Chem. Mater.* **2000**, *12*, 2819.
(11) Kwan, S.; Kim, F.; Akana, J.; Yang, P. D. *Chem. Commun.* **2001**, *5*, 447.
(12) Hu, Y. S.; Zhuang, W. D.; Ye, H. Q.; Wang, D. H.; Zhang, S. S.; Huang, X. W. *J. Alloys Compd.* **2005**, *390*, 226.
(13) Wang, Z. L.; Liang, H. B.; Wang, J.; Gong, M. L.; Su, Q. *Appl. Phys. Lett.* **2006**, *89*, 071921.
(14) Van Vliet, J. P. M.; Blasse, G.; Brixner, L. H. *J. Solid State Chem.* **1988**, *76*, 160.
(15) Yamamoto, H.; Seki, S.; Ishiba, T. *J. Solid State Chem.* **1991**, *94*, 396.
(16) Yan, S.; Zhang, J.; Zhang, X.; Lu, S.; Ren, X.; Nie, Z.; Wang, X. *J. Phys. Chem. C* **2007**, *111*, 13256.
(17) Wang, Z. L.; Liang, H. B.; Gong, M. L.; Su, Q. *Electrochem. Solid-State Lett.* **2005**, *8*, H33.